Materials Innovations

HΣXA Publishers

Catalytic Materials | Research Article | http://doi.org/10.54738/MI.2022.2303

Tin Oxide Supported on Nanostructured MnO_2 as Efficient Catalyst for Nitrophenol Reduction: Kinetic Analysis and Their Application as Heterogeneous Catalyst

Ata Ullah[1], Lutfur Rahman[1], Syed Zajif Hussain[2], Muhammad Bilal Yazdani[1], Asim Jilani[3], Dayum Iqbal Khan[1], Musadiq Zeshan Nasir[1], Waheed S Khan[1], Irshad Hussain[2], Asma Rehman[1]*

1 National Institute for Biotechnology and Genetic Engineering (NIBGE); Constituent College Pakistan Institute of Engineering and Applied Sciences, Faisalabad, 38000, Pakistan
2 Department of Chemistry and Chemical Engineering, SBA School of Science & Engineering (SBASSE), Lahore University of Management Sciences (LUMS), DHA, Lahore Cantt54792, Pakistan
3 Center of Nanotechnology, King Abdul Aziz University, Jeddah, 21589, Saudi Arabia

OPEN ACCESS

This article is part of the special issue on "Women in Materials Science"

Received: 21 January 2022

Accepted: 26 February 2022

Published: 30 March 2022

Editor(s): Sarish Rehman

Citation: Ullah A, Rahman L, Zajif Hussain S, Bilal Yazdani M, Jilani A, Iqbal Khan D, Zeshan Nasir M, Khan WS, Hussain I, Rehman A (**2022**) Tin Oxide Supported on Nanostructured MnO_2 as Efficient Catalyst for Nitrophenol Reduction: Kinetic Analysis and Their Application as Heterogeneous Catalyst. *Materials Innovations 2* (3), 83-91.

***Correspondence**: (Asma Rehman) asmanano@gmail.com

Copyright: © 2022 Ullah A, Rahman L, Zajif Hussain S, Bilal Yazdani M, Jilani A, Iqbal Khan D, Zeshan Nasir M, Khan WS, Hussain I, Rehman A. This is an open access article distributed under the terms of the Creative Commons Attribution License, which permits unrestricted use, distribution, and reproduction in any medium, provided the original author and source are credited.

Published By Hexa Publishers

ISSN
Material 2770-1662

Recently, metal oxides-based nanomaterials have been widely used for catalytic reduction of nitro-aromatic compounds, which are notorious for their carcinogenic nature. The current study reports Sn-doped MnO_2 as an efficient catalyst for the reduction of 4-nitrophenol (4-NP) to 4-aminophenol (4-AP). The FE-SEM characterization of SnO_2-doped MnO_2 revealed the diffused flower-like morphology. Further, the XPS survey scans were performed to investigate the binding energies, oxidation states, and elemental compositions of both MnO_2 and Sn-doped MnO_2. Kinetics analysis revealed that the catalytic reduction (> 98.8%) of 4-NP into 4-AP by Sn-doped MnO_2 in the presence of $NaBH_4$ occurs within four min, following pseudo-first order kinetics. Importantly, no observable deactivation of catalytic efficiency was noticed even after five cycles. Our strategy of loading SnO_2 on the surface of semiconductor nanostructures offers a versatile approach to enhance the catalytic performance, stability, and recyclability which may further promote their practical industrial application.

Keywords: Industrial effluent, Carcinogenic, Catalytic reduction, Sn doped MnO2, 4-Nitrophenol

INTRODUCTION

Advancement in metal oxides-based nanomaterials have garnered their application in several fields, including catalysis.[1] Metal oxides are used for the development of various catalysts due to their unique physico-chemical properties such as high stability, multiple active-sites, and large surface-area. Such nano-catalysts have sufficient bandgap to catalyze several chemical

reactions.[2] Among these metal oxides, manganese dioxide (MnO_2) is considered as a promising material for designing the catalysts for efficient reduction of aro matic compounds, such as 4-Nitrophenol (4-NP). It is because of their relative abundance, environmental compatibility, high surface-reactivity and chemical stability.[3] Morphology of such materials can be tuned into various shapes, such as nanosphere[4], nanowires[5], and nanotubes[6], etc.

However, their catalytic activity has been restricted due to the fast recombination of electron-hole pairs (ehp).[7] Further, metal oxide nanoparticles (NPs) can agglomerate with each other and remain unstable due to their high-surface energy. In addition, from the reaction mixture, these NPs cannot be easily separated and thus difficult to recycle. Therefore, numerous efforts have been made to stabilize metal oxide NPs to prevent their agglomeration and enhance their stability/recyclability.[8] Surface-capping of metal oxides NPs effectively prevent their agglomeration and maintain their stability. Similarly, these NPs may be loaded on supporting materials to design heterogeneous catalysts that exhibit high catalytic activity and are easier to recycle and reuse.[9] Another approach is doping, which is the most promising, and give multiple properties of two or more NPs in a single composite resulting in extraordinary catalytic activity, stability, and recyclability.[10]

The current study reports a convenient and facile approach for the synthesis of Sn-doped MnO_2 based heterogeneous catalysts with unique morphology and proficient catalytic activity. Tin-oxide (SnO_2) is an n-type metal oxide semiconductor that exhibits high carrier density, oxygen vacancy, and chemical stability. Due to these properties, it can potentially catalyze several reactions in an environmental interest.[11] Therefore, Sn-doped MnO_2-based composite may have an excellent interface to prevent ehp recombination. The possible reason behind it could be the creation of surface defects and oxygen vacancies on the surface of SnO_2. Thus, increasing in the catalytic performance, stability and recyclability of the designed hybrid catalyst.[11,12]

On the other hand, rapid industrialization has led to the contamination of water which is not only vital for human survival but also necessary for sustainable agriculture.[13] Effluents from several, chemical, pharmaceutical, pulp/paper and tannery industries are frequently being discharged into aquatic bodies without prior treatment, which causes severe environmental concerns.[14] These effluents contain heavy metals, recalcitrant dyes and other aromatic compounds.[15] Among them, 4-NP is an essential precursor in the synthesis of synthetic dyes, paint, pesticides, herbicides explosive, drugs, wood preservatives, etc.[16] Therefore, effluents discharged from these chemical industries are contaminated with 4-NP, which is highly carcinogenic for animals and induces toxicity in living tissues via the redox process.[17] Therefore, the detoxification of 4-NP in aqueous bodies via reduction into their lesser toxic counterpart has significantly attracted the global interests.[17]

To address the above-mentioned environmental challenges, we report a facile hydrothermal approach for the synthesis of Sn-doped MnO_2 hybrid composite, as a promising catalyst for 4-NP reduction. The as-synthesized catalyst has been characterized through Field-Emission Scanning Electron Microscope (FE-SEM) and X-ray Photoelectron Spectroscopy (XPS). Their catalytic efficiency has been measured spectrophotometrically at different concentrations of 4-NP and sodium borohydride ($NaBH_4$). Additionally, the recyclability of Sn-doped MnO_2 catalyst has also been checked for 5-cycles that demonstrate its excellent potential for recyclability and reusability.

EXPERIMENTAL SETUP

All analytically grade chemicals i.e., potassium permanganate ($KMnO_4$) 98+ % from ACROS, anhydrous Tin (IV) chloride ($SnCl_2.4H_2O$) 98 % from Alfa Aesar, ethanol (absolute), hydrochloric acid (37 %) from Sigma-Aldrich, hydrogen peroxide (H_2O_2), and poly (vinyl)alcohol (PVA) were purchased from ACROS. All the solutions were prepared in deionized water (ρ = 18 MΩ cm from the Millipore Milli-Q system.

Synthesis of Manganese dioxide nanostructures

Manganese dioxide (MnO_2) nanostructures were synthesized by modifying the previously reported method.[18] In a typical experiment, 0.048 g of $KMnO_4$ was added into 50 mL of HNO_3 (1.3M). After 30 min magnetic stirring, the solution was transferred to a Teflon-lined autoclave and hydrothermally treated at 80 °C for 5 hours. The product was recovered through centrifugation (3000 rpm), and washed several times with ethanol, and deionized water sequentially. Then, the prepared catalysts were vacuum dried at 60 °C overnight and stored in a desiccator for further use.

Synthesis of Sn-doped MnO_2 nanocomposites

For the synthesis of Sn-doped MnO_2, as-synthesized MnO_2 nanostructures were allowed to a second low-hydrothermal treatment in the presence of $SnCl_2.4H_2O$ ranging from 1:1 to 1:9 Sn/Mn atomic weight ratios.[19] Briefly, a specific amount of thoroughly sonicated MnO_2 nanostructures were added to 20 mL acidic solution (0.7 mL of 38%) of $SnCl_2.4H_2O$ (0.15 g). The mixture was magnetically stirred for 30 min. Then, transferred it to 100 mL Teflon-lined stainless-steel autoclave followed by hydrothermal treatment at 90 °C for 5 hours. The

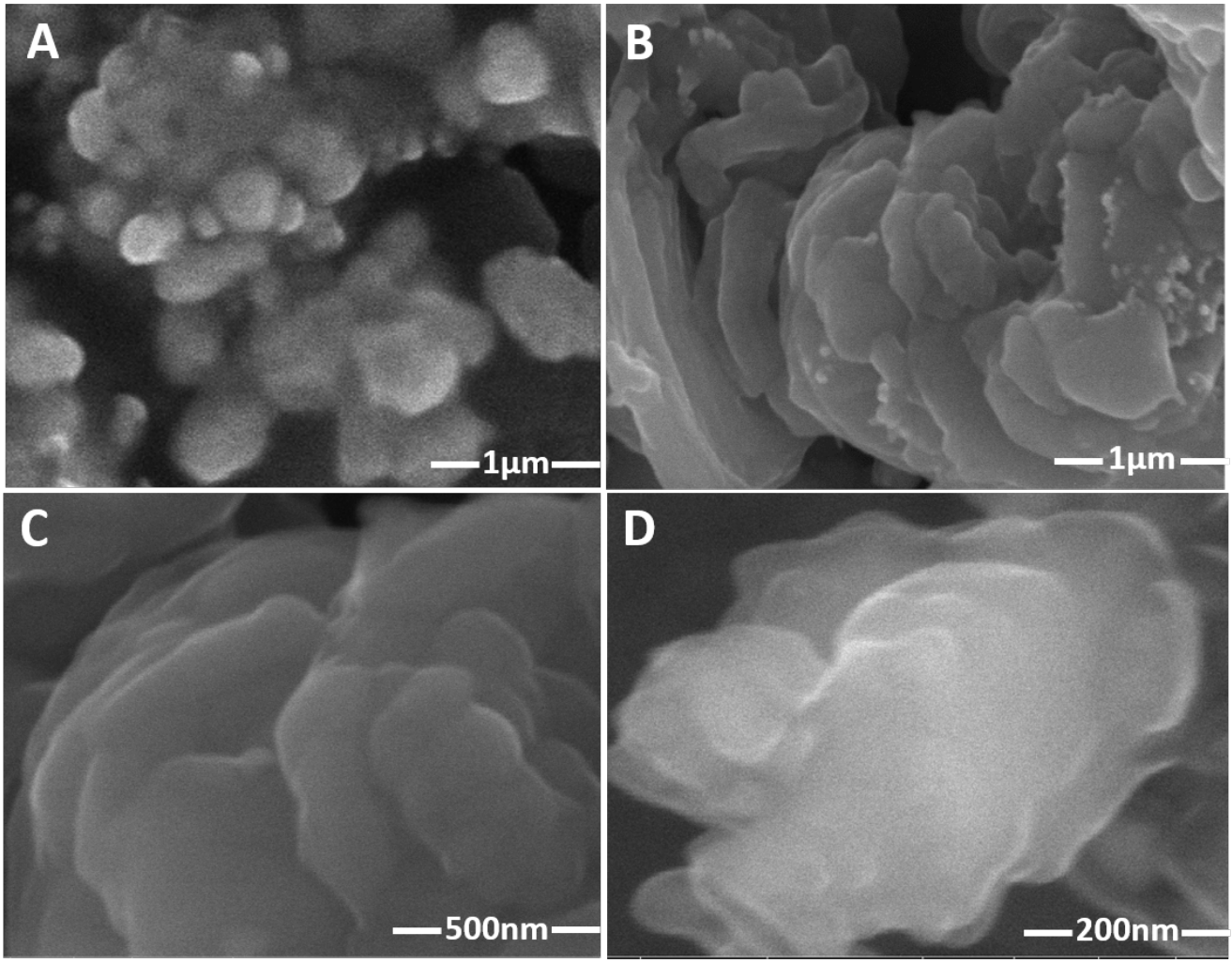

Figure 1. Field emission scanning electron micrograph of the designed catalyst (a) MnO_2 NPs. (b, c, d) Sn-doped MnO_2 morphologies at different resolutions.

as-synthesized Sn-doped MnO_2 were recovered through centrifugation, vacuum dried at 70 °C and stored in a desiccator for further studies.

The morphology of the synthesize nanomaterials were explored through Field Emission-Scanning Electron Microscopy (FE-SEM). Further, the compositional information and binding energy of Sn-doped MnO_2 were determined through X-ray Photoelectron spectroscopy (XPS).

Catalytic study

The catalytic activities of both MnO_2 nanostructure and Sn-doped MnO_2 were investigated using 4-NP as a model pollutant. In a typical reaction, 2.7 mL of 4-NP (0.1 mM) was mixed with 0.3 mL of freshly prepared $NaBH_4$ (0.1 M), followed by the addition of catalyst in the range of 1-5 mg mL^{-1} under optimized reaction conditions at room temperature. The catalytic reduction of the 4-NP was spectrophotometrically monitored in the range of 200-700 nm with respect to time (t). The recyclability of as-synthesized catalyst was also checked as follows: once the reaction was completed, the catalyst was recovered through centrifugation, washed with 10 % ethanol solution, and vacuum dried at 70 °C for 5-6 h. The dried catalysts were then again used for the subsequent reactions to check their reusability and stability.

RESULTS AND DISCUSSION

The reduction kinetics of 4-NP were calculated from the UV-Vis absorption spectra of the reaction solution, which reveal that the reduction kinetics follow pseudo-first-order. Pseudo-first-order kinetics can be described as $ln\ (Ct/Co)$ where C_o and C_t are the concentrations of 4-AP at time zero and t, respectively. The $ln\ (C_t/C_o)$ was

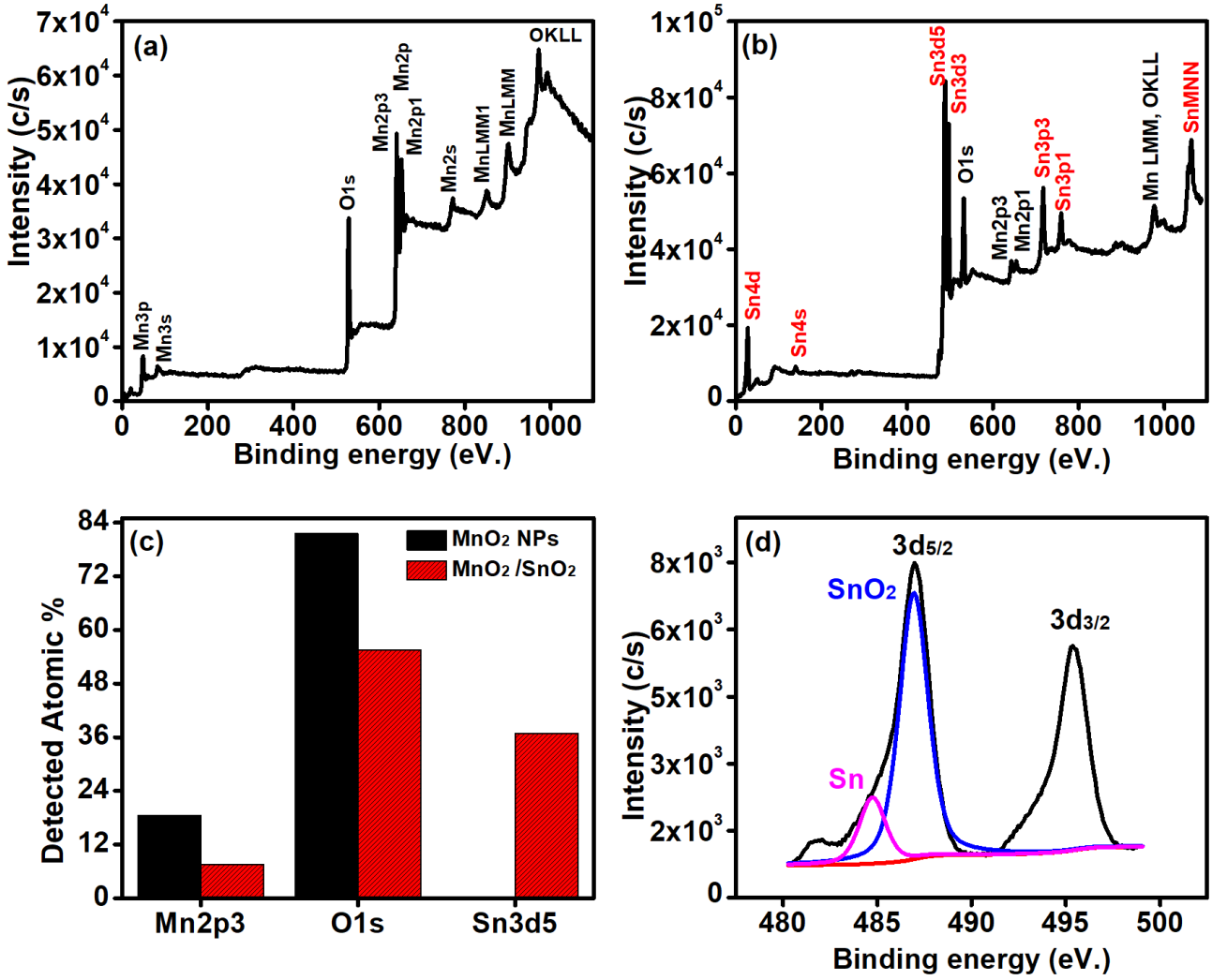

Figure 2. (a-c) Survey scan and compositional analysis of MnO_2 and Sn-doped MnO_2, while (d) Sn3d5 analysis of Sn-doped MnO_2.

plotted against reaction time (t), which exhibited the best linear correlation ($R^2 > 0.996$) as shown in Figure 5(a). The rate constant (K_{app}) was calculated from the slope of $ln(C_t/C_o)-t$, which revealed that the Sn-doped MnO_2 had efficient catalytic reduction activity with $K_{app} > 4.7884\ min^{-1}$ as compared to MnO_2 alone ($K_{app} = 0$).

The FE-SEM morphology of MnO_2 showed their diffused flower-like morphology as shown in Figure 1(a). Such flower-like morphology for MnO_2 has also been reported by Rivera-Lugo and co-workers.[18] Our study shows that at low hydrothermal temperature and lesser treatment time (5-6 h), MnO_2 exhibits flower-like morphology. However, at high temperature and longer treatment time, the flower-like morphology transforms into rod-like structures. The FE-SEM micrograph of Sn-doped MnO_2 shows flower-like morphology, which is comprised of large, thick petal-like layers (Figure 1 (b-d)). This may indicate that second-low hydrothermal treatment of MnO_2 in the presence of Tin (IV) chloride (acidic condition) has improved their diffused flower-like morphology with well-defined, large and thick layers, like petals. Such transformation in morphology has also been demonstrated by Lan and co-workers.[20] Zhao et al have further explained that the flower-like morphology provides large surface area and enhance catalyst's activities. Further reported that catalysts with flower-like morphology possesses more atoms at the edges and corners, thus provides more active sites for the interactions with reactants.[21]

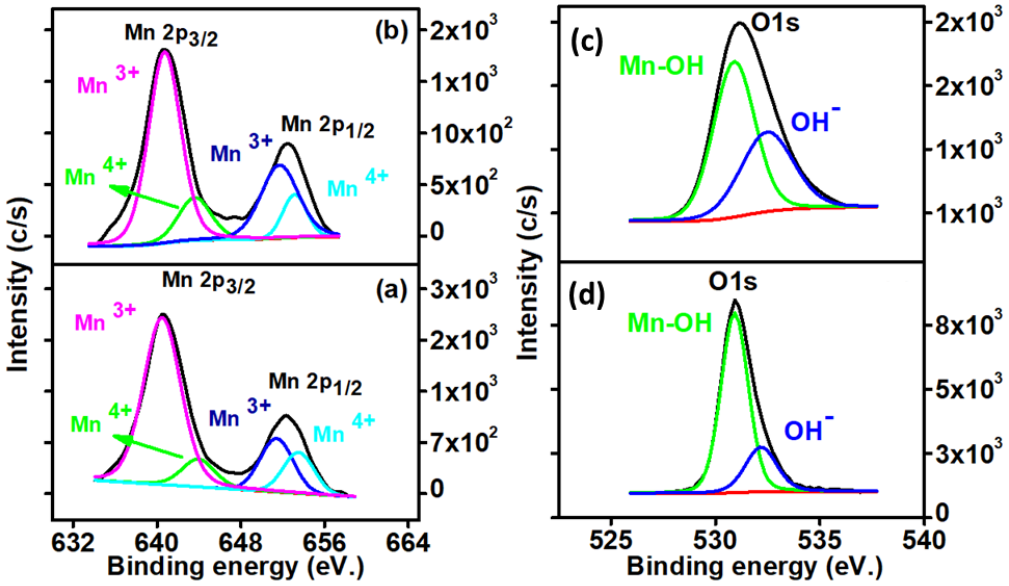

Figure 3. Mn2p analysis for (a) MnO_2 nanostructures (b) Sn-doped MnO_2 (c-d) O1s functional groups analysis for (c) MnO_2 nanostructures and (d) Sn-doped MnO_2.

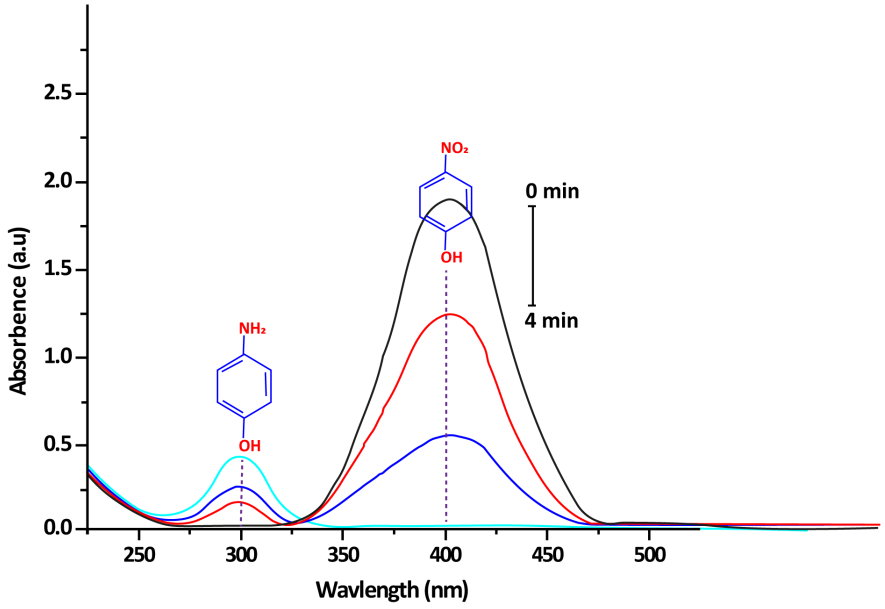

Figure 4. UV-Vis absorption spectra of the catalytic reduction of 4-NP in the presence of Sn-doped MnO_2, using $NaBH_4$ as electrons donor.

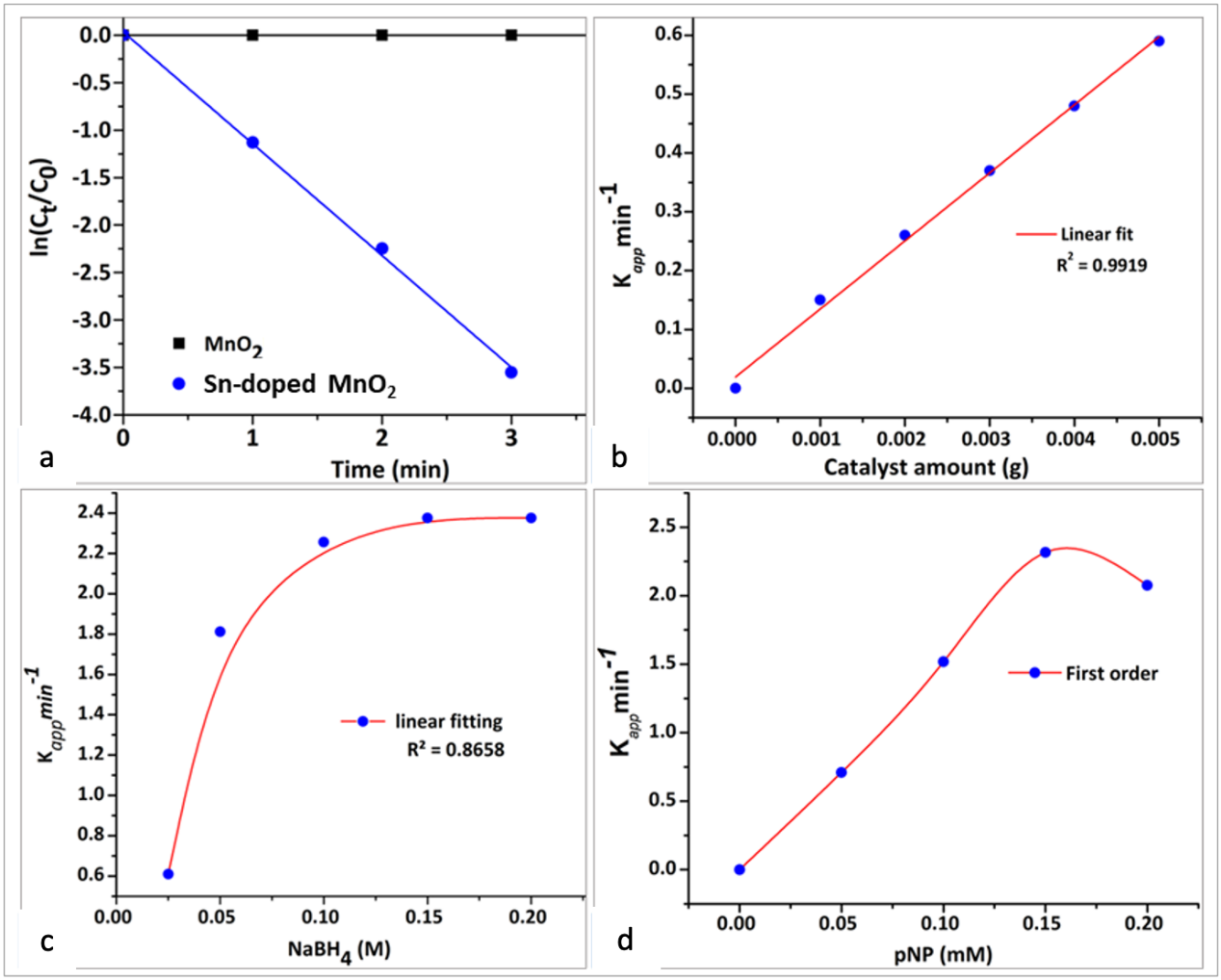

Figure 5. (a) Plot of ln (C_t/C_o)against the reaction time 't' for MnO_2, Sn-doped MnO_2 under 1M $NaBH_4$, 0.1mM 4-NP, respectively at room temperature, (b) Plot of K_{app} against amount of Sn-doped MnO_2 under optimized conditions, (c, d) are the effect of 4-NP and $NaBH_4$ concentrations on the rate constant K_{app}.

The surface compositions of as-synthesized MnO_2 nanostructures and Sn-doped MnO_2were investigated using XPS. The survey scan of MnO_2 nanostructure revealed the presence of Mn2p3 (18.5 %) and O1s (81.5%) without any residual impurities (Figure 2(a)). Further, the survey scan of Sn-doped MnO_2 (Figure 2(b)) confirms the presence of Sn3d5 (36.9%) along with Mn2p3 (7.6%) and O1s (55.5%). The graphical representation of each detected element of MnO_2 nanostructure and Sn-doped MnO_2 is shown in Figure 2(c).

Moreover, the chemical state analysis of Sn3d5, Mn2p3 and O1s were performed to determine the functional groups. The Sn3d5 analysis of Sn-doped MnO_2 (Figure 2(d)), Sn3d5 has two peaks around 486.97 eV and 495.47 eV that are attributed to the 3d5/2 and 3d/3/2, respectively. Further, the difference between these two peaks were noticed around 8.5 eV. Moreover, the peak fitting of 3d5/2 disclosed the manifestation of two peaks around 484.74 eV and 486.94 eV, which is recognized as SnO_2 and Sn in metallic form.[22] Moreover, the contribution of SnO_2 was around 81.34 %, while 18.66% for Sn metallic.

Mn2p analysis for MnO_2 nanostructures show (Figure 3(a)) the appearance of two main peaks around 640.50 and 651.41 eV which are attributed to the 2p3/2 and 2p1/2, respectively. Further, the peak fitting of 2p3/2 and 2p1/2 revealed four peaks around 640.49 eV, 643.95, 651.41 and 653.50 eV respectively for Mn3+, Mn4+ (2p3/2) and Mn3+, Mn4+ (2p1/2).22 Moreover, a change in Mn^{3+} and Mn^{4+} was observed after the addition of SnO_2 (Figure 3(b)).

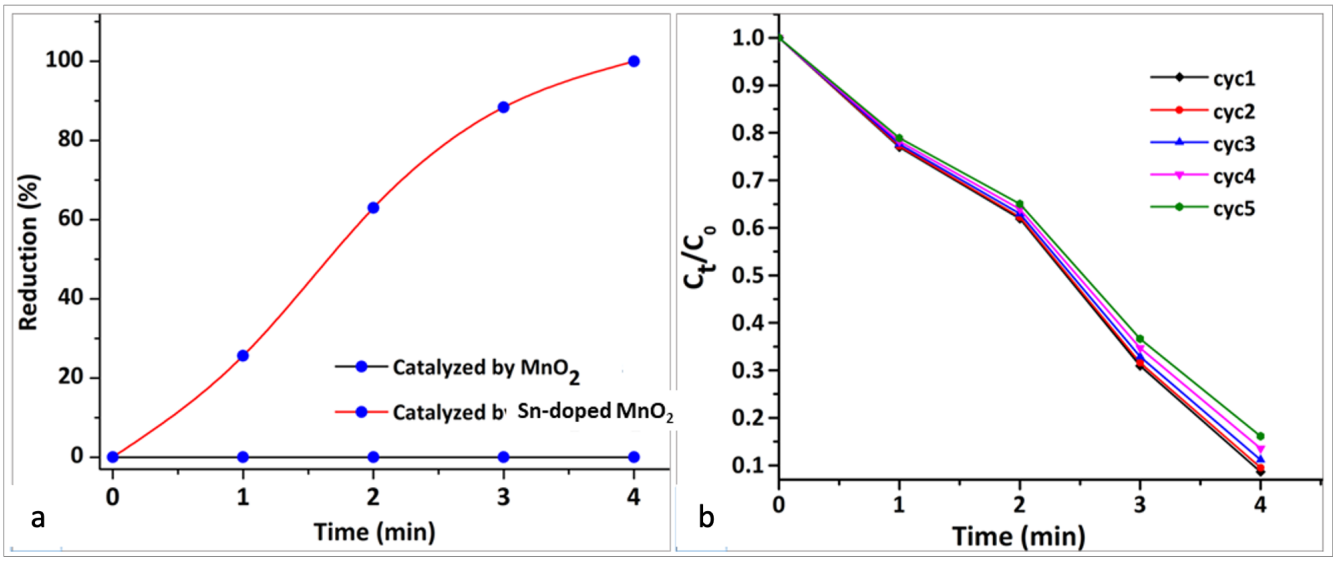

Figure 6. (a) Plot of 4-NP % reduction against reaction time; (b) recyclability and reusability properties of the Sn-doped MnO_2 catalyst under optimized reaction condition.

O1s spectra of MnO_2 nanostructures (Figure 3(c)) show the presence of two peaks around 530.90 eV and 532.3 eV, which are attributed to Mn-OH and OH^-, respectively. The contribution of Mn-OH changed from 76.80 % to 60.70 % with the addition of Sn to MnO_2 (Figure 3(d)).[23−24]However, an increase in the $OH^-$was noticed from 23.20 % to 39.30 % is favorable for the enhanced catalytic activity of these materials.25

The catalytic activity of the Sn-doped MnO_2 was explored for the reduction of 4-NP into 4-aminophenol (4-AP), using sodium borohydride ($NaBH_4$) as a source of electron donor. Catalytic reduction of 4-NP was monitored by UV-Vis absorption spectra of the solution (Figure 4). A maximum absorption spectrum of 4-NP ions in solution was recorded at 400 nm, when $NaBH_4$ was added to the 4-NP solution. Once, the Sn-doped MnO_2 catalyst was added to 4-NP solution, a significant decrease was observed in the intensity of absorption peak at 400 nm, while an increase in absorption peak at 300 nm was recorded that indicates the conversion of 4-NP to 4-AP. Moreover, the catalytic reduction was also observed visually by observing the fading of the greenish color of 4-NP solution to transparent.[26] As-synthesized Sn-doped MnO_2 catalysts have shown excellent reduction activity and completed the reduction within 4 minutes, however MnO_2 nanostructures haven't shown significant catalytic activity. Thus, the best catalytic activity of Sn-doped MnO_2 is due to the synergisticeffect of both metal oxides, namely SnO_2 and MnO_2. The reported literature has mentioned that Sn-doping on MnO_2 heterostructure may decreases their bandgap. Due to which the electrons are easily ejected for MnO_2 to produced electron-hole pairs that impart proficient catalytic activity to Sn-doped MnO_2 catalyst.[27]

Further, the 4-NP reduction kinetics were explored at different reaction conditions. The amount of Sn-doped $MnO_2$was changed in the range of 1-5 mg, while keeping $NaBH_4$ (1 M) and 4-NP (0.1 mM) concentrations constant. Under these optimized conditions, the K_{app} increased linearly with increasing the amount of catalyst (Figure 5(b)). It is obvious, that increase in catalyst amount provide more active sites for the reduction process. In the case of increasing $NaBH_4$ concentration from 0.025 to 0.1 M, an increase in K_{app} occurred; though no change in K_{app} was observed when the concentration increased from 0.15 M to 0.2 M (Figure 5(c)). Similarly, the effect of 4-NP concentration (0.05-0.2 mM) was investigated, and the results are shown in Figure 5(d). The K_{app} increases as the 4-NP concentration increases from 0.05 to 0.15 mM, but beyond 0.15 mM concentration K_{app} decreases. However, these nonlinear relationships between K_{app} with $NaBH_4$, along with a fall in K_{app} by increasing the 4-NP concentration shows that both reactants compete with each other on the surface of Sn-doped MnO_2 catalyst. Similar relation between rate constant and nitrophenol concentration was documented by Mona and Reza Gholami, using CeO_2 nanorods supported on CuNi nanoparticles.[28]

The percent (%) reduction of 4-NP to 4-AP by the as-synthesized catalysts in the presence of $NaBH_4$ were calculated using the equation; $\eta = 1 - C_t/C_o \times 100$ (Figure 6(a)),[29] which showed > 98% reduction of 4-NP into 4-AP within 4 min. The recyclability and reusability of Sn-doped MnO_2 were checked for five consecutive cycles under optimized conditions (4-NP (0.1 mM), 0.1 M $NaBH_4$ at RT)

(Figure 4(b)). The results showed that in each consecutive cycle the reduction time increases slightly i.e., up to 15-30 sec, that might be due to the minute loss of catalyst during recovery processing (centrifugation, washing and drying).[30]

CONCLUSIONS

A facile hydrothermal approach was used for the synthesis of hybrid Sn-doped MnO_2 catalyst. The flower-like morphology of Sn-doped MnO_2 with diffused petals showed that the deposition of specific amount of Sn on MnO_2 nanostructure has improved the petal-like layers of MnO_2. XPS study confirmed that the Mn-OH reduced from 76.80 % to 60.70 % due to the addition of Sn on MnO_2, which depict the successful deposition of Sn on MnO_2 nanostructure. The pure MnO_2 nanostructures were found catalytically inactive but the designed Sn-doped MnO_2 have reduced 4-NP into 4-AP (>98.8%) only in four minutes with high catalytic activity even after five cycles, thus demonstrating their effective reusability.

ACKNOWLEDGMENTS

The authors declare not conflict of interest.This study was funded by the Higher Education Commission (HEC) of Pakistan under the head of NRPU Project # 6118). The Principal investigator (PI) of this project was; Dr. Asma Rahman, Senior scientist at National Institute of Biotechnology and Geneticengineering (NIBGE), Faisalabad. The authors highly acknowledge the financial support of the HEC, Pakistan.

References

1) Barua, R.; Datta, S.; Das, J. Application of Nanotechnology in Global Issues. *Advances in Human Services and Public Health* **2020**, 292–300.
2) Narayan, N.; Meiyazhagan, A.; Vajtai, R. Metal Nanoparticles as Green Catalysts. *Materials* **2019**, *12* (21), 3602–3602, DOI: 10.3390/ma12213602, available at https://dx.doi.org/10.3390/ma12213602.
3) Chiam, S.-L.; Pung, S.-Y.; Yeoh, F.-Y. Recent developments in MnO2-based photocatalysts for organic dye removal: a review. *Environmental Science and Pollution Research* **2020**, *27* (6), 5759–5778, DOI: 10.1007/s11356-019-07568-8, available at https://dx.doi.org/10.1007/s11356-019-07568-8.
4) Srither, S. R.; Karthik, A.; Murugesan, D.; Arunmetha, S.; Selvam, M.; Rajendran, V. Electrochemical capacitor study of spherical MnO2 nanoparticles utilizing neutral electrolytes. *Frontiers in Nanoscience and Nanotechnology* **2015**, *1* (1), 13–20, DOI: 10.15761/fnn.1000103, available at https://dx.doi.org/10.15761/fnn.1000103.
5) Tehseen, B.; Rehman, A.; Rahmat, M.; Bhatti, H. N.; Wu, A.; Butt, F. K.; Naz, G.; Khan, W. S.; Bajwa, S. Z. Solution growth of 3D MnO2 mesh comprising 1D nanofibres as a novel sensor for selective and sensitive detection of biomolecules. *Biosensors and Bioelectronics* **2018**, *117*, 852–859, DOI: 10.1016/j.bios.2018.06.061, available at https://dx.doi.org/10.1016/j.bios.2018.06.061.
6) Chalkidis, A.; Jampaiah, D.; Amin, M. H.; Hartley, P. G.; Sabri, Y. M.; Bhargava, S. K. CeO2-Decorated?-MnO2 Nanotubes: A Highly Efficient and Regenerable Sorbent for Elemental Mercury Removal from Natural Gas. *Langmuir 2019* (25), 8246–8256.
7) Khan, M. A.; Nadeem, M. A.; Idriss, H. Ferroelectric polarization effect on surface chemistry and photo-catalytic activity: A review. *Surface Science Reports* **2016**, *71* (1), 1–31, DOI: 10.1016/j.surfrep.2016.01.001, available at https://dx.doi.org/10.1016/j.surfrep.2016.01.001.
8) Cartwright, A.; Jackson, K.; Morgan, C.; Anderson, A.; Britt, D. W. A Review of Metal and Metal-Oxide Nanoparticle Coating Technologies to Inhibit Agglomeration and Increase Bioactivity for Agricultural Applications. *Agronomy* **2020**, *10* (7), 1018–1018, DOI: 10.3390/agronomy10071018, available at https://dx.doi.org/10.3390/agronomy10071018.
9) Ma, H.-C.; Kan, J.-L.; Chen, G.-J.; Chen, C.-X.; Dong, Y.-B. Pd NPs-Loaded Homochiral Covalent Organic Framework for Heterogeneous Asymmetric Catalysis. *Chemistry of Materials* **2017**, *29* (15), 6518–6524, DOI: 10.1021/acs.chemmater.7b02131, available at https://dx.doi.org/10.1021/acs.chemmater.7b02131.
10) Yang, Y.; Luo, S.; Guo, S.; Chao, Y.; Yang, H.; Li, Y. Synthesis of Au nanoparticles supported on mesoporous N-doped carbon and its high catalytic activity towards hydrogenation of 4-nitrophenol to 4-aminophenol. *International Journal of Hydrogen Energy* **2017**, *42* (49), 29236–29243, DOI: 10.1016/j.ijhydene.2017.10.086, available at https://dx.doi.org/10.1016/j.ijhydene.2017.10.086.
11) Periyasamy, M.; Kar, A. Modulating the properties of SnO2 nanocrystals: morphological effects on structural, photoluminescence, photocatalytic, electrochemical and gas sensing properties. *Journal of Materials Chemistry C* **2020**, *8* (14), 4604–4635, DOI: 10.1039/c9tc06469a, available at https://dx.doi.org/10.1039/c9tc06469a.
12) Shao, M.; Liu, J.; Ding, W.; Wang, J.; Dong, F.; Zhang, J. Oxygen vacancy engineering of self-doped SnO2 nanocrystals for ultrasensitive NO2 detection. *Journal of Materials Chemistry C* **2020**, *8* (2), 487–494, DOI: 10.1039/c9tc05705f, available at https://dx.doi.org/10.1039/c9tc05705f.
13) Kilic, Z. The importance of water and conscious use of water. *Int J Hydro 2020* (5), 239–241.
14) SI, B.; JM, R.; NF, B.; VSG, G.; AL, S. Emerging pollutants, related toxicity, and water quality decreasing: tannery, textile, and pharmaceuticals load pollutants. *Biology, Engineering and Medicine* **2018**, *3* (6), DOI: 10.15761/bem.1000157, available at https://dx.doi.org/10.15761/bem.1000157.
15) Singh, R. L.; Singh, R. P. 2019.
16) Zhang, K.; Suh, J. M.; Choi, J.-W.; Jang, H. W.; Shokouhimehr, M.; Varma, R. S. Recent Advances in the Nanocatalyst-Assisted NaBH4 Reduction of Nitroaromatics in Water. *ACS Omega* **2019**, *4* (1), 483–495, DOI: 10.1021/acsomega.8b03051, available at https://dx.doi.org/10.1021/acsomega.8b03051.
17) Feng, Y.; Yin, J.; Liu, S.; Wang, Y.; Li, B.; Jiao, T. Facile Synthesis of Ag/Pd Nanoparticle-Loaded Poly(ethylene imine) Composite Hydrogels with Highly Efficient Catalytic Reduction of 4-Nitrophenol. *ACS Omega* **2020**, *5* (7), 3725–3733, DOI: 10.1021/acsomega.9b04408, available at https://dx.doi.org/10.1021/acsomega.9b04408.
18) Zahoor, A.; Jeon, J. S.; Jang, H. S.; Christy, M.; Hwang, Y.; Nahm, K. S. Mechanistic Study on Phase and Morphology Conversion of MnO2 Nanostructures Grown by Controlled Hydrothermal Synthesis. *Science of Advanced Materials* **2014**, *6* (12), 2712–2723, DOI: 10.1166/sam.2014.1990, available at https://dx.doi.org/10.1166/sam.2014.1990.
19) Ullah, A.; Rahman, L.; Hussain, S. Z.; Abbas, W.; Tawab, A.; Jilani, A.; Bajwa, S. Z.; Khan, W. S.; Riaz, R.; Hussain, I.; Rehman, A. Mechanistic insight of dye degradation using TiO2 anchored α-MnO2 nanorods as promising sunlight driven photocatalyst. *Materials Science and Engineering: B* **2021**, *271*, 115257–115257, DOI: 10.1016/j.mseb.2021.115257, available at https://dx.doi.org/10.1016/j.mseb.2021.115257.
20) Lan, B.; Huang, S.; Ye, C.; Qin, Q.; Yan, J.; Wu, Y. Enhanced electrochemical performance of Sn-doped MnO2 and study on morphology evolution. *Journal of Alloys*

and Compounds **2019**, *788*, 302–310, DOI: 10.1016/j.jallcom.2019.02.171, available at https://dx.doi.org/10.1016/j.jallcom.2019.02.171.

21) Nisha, K. D.; Navaneethan, M.; Dhanalakshmi, B.; Hayakawa, Y.; Ponnusamy, S.; Muthamizhchelvan, C. Formation and morphological investigation of petal-like cadmium sulphide nanostructures. *Optical Materials* **2013**, *35* (9), 1652–1658, DOI: 10.1016/j.optmat.2013.04.020, available at https://dx.doi.org/10.1016/j.optmat.2013.04.020.
22) Moulder, J. F. Handbook of X-Ray Photoelectron Spectroscopy. *Physical Electronics* **1995**, 230–232.
23) Xu, C.; Shi, S.; Sun, Y.; Chen, Y.; Kang, F. Ultrathin amorphous manganese dioxide nanosheets synthesized with controllable width. *Chemical Communications* **2013**, *49* (66), 7331–7331, DOI: 10.1039/c3cc43055c, available at https://dx.doi.org/10.1039/c3cc43055c.
24) Gubbala, S.; Russell, H. B.; Shah, H.; Deb, B.; Jasinski, J.; Rypkema, H.; Sunkara, M. K. Surface properties of SnO2 nanowires for enhanced performance with dye-sensitized solar cells. *Energy & Environmental Science* **2009**, *2* (12), 1302–1302, DOI: 10.1039/b910174h, available at https://dx.doi.org/10.1039/b910174h.
25) Jilani, A.; Rehman, G. U.; Ansari, M. O.; Othman, M. H. D.; Hussain, S. Z.; Dustgeer, M. R.; Darwesh, R. Sulfonated polyaniline-encapsulated graphene@graphitic carbon nitride nanocomposites for significantly enhanced photocatalytic degradation of phenol: a mechanistic study. *New Journal of Chemistry* **2020**, *44* (45), 19570–19580, DOI: 10.1039/d0nj03684f, available at https://dx.doi.org/10.1039/d0nj03684f.
26) Raza, W.; Krupanidhi, S. B. Engineering Defects in Graphene Oxide for Selective Ammonia and Enzyme-Free Glucose Sensing and Excellent Catalytic Performance for para-Nitrophenol Reduction. *ACS Applied Materials & Interfaces* **2018**, *10* (30), 25285–25294, DOI: 10.1021/acsami.8b05162, available at https://dx.doi.org/10.1021/acsami.8b05162.
27) Panimalar, S.; Subash, M.; Chandrasekar, M.; Uthrakumar, R.; Inmozhi, C.; Al-Onazi, W. A.; Al-Mohaimeed, A. M.; Chen, T.-W.; Kennedy, J.; Maaza, M.; Kaviyarasu, K. Reproducibility and long-term stability of Sn doped MnO2 nanostructures: Practical photocatalytic systems and wastewater treatment applications. *Chemosphere* **2022**, *293*, 133646–133646, DOI: 10.1016/j.chemosphere.2022.133646, available at https://dx.doi.org/10.1016/j.chemosphere.2022.133646.
28) Kohantorabi, M.; Gholami, M. R. Kinetic Analysis of the Reduction of 4-Nitrophenol Catalyzed by CeO2 Nanorods-Supported CuNi Nanoparticles. 2017; available at https://dx.doi.org/10.1021/acs.iecr.6b04208.
29) Qi, B.; Wu, C.; Liu, Y.; Liu, J.; Zhang, H. Self-Assembled Magnetic Pt Nanocomposites for the Catalytic Reduction of Nitrophenol. *ACS Applied Nano Materials* **2019**, *2* (7), 4377–4385, DOI: 10.1021/acsanm.9b00794, available at https://dx.doi.org/10.1021/acsanm.9b00794.
30) Mohamed, M. J. S.; Denthaje, K. B. Novel RGO-ZnWO4Fe3O4 Nanocomposite as an Efficient Catalyst for Rapid Reduction of 4-Nitrophenol to 4-Aminophenol. *Industrial & Engineering Chemistry Research* **2016**, *55* (27), 7267–7272, DOI: 10.1021/acs.iecr.6b01882, available at https://dx.doi.org/10.1021/acs.iecr.6b01882.